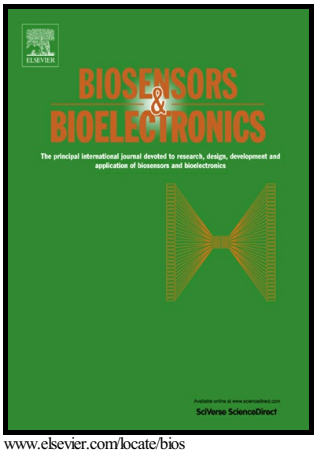

www.elsevier.com/locate/bios

A signal-decreased electrochemical immunosensor for the sensitive detection of LAG-3 protein based on a hollow nanobox-MOFs/AuPt alloy

Wei Xu, Zhen Qin, Yutong Hao, Qiang He, Shuai Chen, Zhongshuang Zhang, Dan Peng, Haiyan Wen, Jun Chen, Jingfu Qiu, Chaorui Li

PII: S0956-5663(18)30349-X
DOI: https://doi.org/10.1016/j.bios.2018.05.010
Reference: BIOS10468

To appear in: *Biosensors and Bioelectronic*

Received date: 12 January 2018
Revised date: 3 May 2018
Accepted date: 7 May 2018

Cite this article as: Wei Xu, Zhen Qin, Yutong Hao, Qiang He, Shuai Chen, Zhongshuang Zhang, Dan Peng, Haiyan Wen, Jun Chen, Jingfu Qiu and Chaorui Li, A signal-decreased electrochemical immunosensor for the sensitive detection of LAG-3 protein based on a hollow nanobox-MOFs/AuPt alloy, *Biosensors and Bioelectronic,* https://doi.org/10.1016/j.bios.2018.05.010

A signal-decreased electrochemical immunosensor for the sensitive detection of LAG-3 protein based on a hollow nanobox-MOFs/AuPt alloy

Wei Xu[1], Zhen Qin[1], Yutong Hao[2], Qiang He[1], Shuai Chen[1], Zhongshuang Zhang[1], Dan Peng[1], Haiyan Wen[2], Jun Chen[1], Jingfu Qiu[*, 1] Chaorui Li[*, 1]

[1]School of Public Health and Management, Chongqing Medical University, Chongqing 400016, China

[2]Chongqing International Travel Health Care Center, Chongqing 401120, China

[*]Corresponding author: Tel & fax: +86-23-68485026, jfqiu@126.com

[*]Co-corresponding author: Tel & fax: +86-23-68485026, crli@cqmu.edu.cn

Abstract:

In this work, hollow nanobox metal-organic framework (HNM) nanocomposites were synthesised and utilised for the first time in a signal decreased electrochemical immunosensor for the ultrasensitive quantitative determination of lymphocyte activation gene-3 (LAG-3) protein, which is a newly discovered biomarker. With the aid of signal materials, namely, SiO_2-tagged anti-LAG-3 antibody (SiO_2-Ab_2) and the biotin-streptavidin system, the sensor can achieve signal amplification. Encapsulation of tin dioxide-functionalised reduced graphene oxide (rGO-SnO_2) and gold and platinum alloys (AuPt alloys) onto the surface of hollow nanobox metal-organic frameworks (MOFs) was performed to prepare rGO-SnO_2/hollow nanobox-MOFs/AuPt alloys (rGO-SnO_2/HNMs/AuPt) as the matrix. SiO_2-Ab_2, which is used as the signal-decreased label, can be utilised to enhance the distinction of the electrochemical signal after the specific recognition between antibodies and antigens, owing to its large steric hindrance property. In this sensor, this proposed sandwich immunosensor can achieve a high sensitivity, especially in the presence of low concentrations of the LAG-3 protein. Under optimal conditions, this sandwich-designed immunosensor exhibited a sensitive detection of the LAG-3 protein from concentrations of 0.01 $ng \cdot mL^{-1}$ to 1 $\mu g \cdot mL^{-1}$, with a lower detection limit of 1.1 $pg \cdot mL^{-1}$ (based on 3σ). We proposed that this ultrasensitive biosensor can be utilised for the detection of the LAG-3 protein in early clinical tumour diagnosis.

Graphical Abstract:

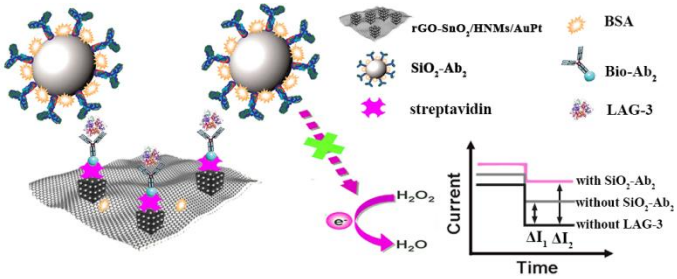

Keywords: Hollow nanobox MOFs; SiO_2 tag antibody; Sandwich electrochemical immunosensor; Lymphocyte activation gene-3; Biotin-streptavidin

1. Introduction

Lymphocyte activation gene-3 (LAG-3) protein is a type I transmembrane protein expressed on activated $CD4^+$ and $CD8^+$ T cells (Workman et al. 2002). As a negative checkpoint inhibitor (Turnis et al. 2015), LAG-3 negatively regulates T-cell function, thereby contributing to tumour escape (Shapiro et al. 2017). A change of LAG-3 concentration may be considered a sign of diseases such as HIV infection (Juno et al. 2015), coronary artery disease (Golden et al. 2016), chronic lymphocytic leukaemia (Jie et al. 2010), melanoma (Legat et al. 2015), renal cell carcinoma, and pancreatic and prostate cancers in humans (Topalian et al. 2012). LAG-3 is a potential tumour biomarker that could be detected earlier than other biomarkers (Andrews et al. 2017). Therefore, the development of LAG-3 protein detection methods with high sensitivity and selectivity is vital for clinical real-time monitoring and early diagnosis of tumours,

in order to decrease the detrimental effects on human health.

According to previous literature, immunoblots (Kim et al. 2010), chemiluminesence (Golden et al. 2016), enzyme-linked immunosorbent assays (ELISA) (Li et al. 2008), and thymidine incorporation assays have been used for LAG-3 protein detection (Xia et al. 2017). These methods can detect LAG-3 protein with high accuracy and robustness. However, these methods require labour, expensive equipment, a long detection time, and sophisticated sample preparation. This restricts the use of these methods for on-site LAG-3 detection. In recent years, electrochemical immunosensors have been used in portable devices and point-of-care applications (Kavosi et al. 2015). Hence, electrochemical immunosensors have been developed and used extensively for the detection of tumour biomarkers, food additives, and environmental pollutants (He et al. 2015; Wang et al. 2017b).

Herein, we reported a sandwich electrochemical immunosensor for the ultrasensitive detection of the LAG-3 protein by encapsulating tin dioxide-functionalised reduced graphene oxide (rGO-SnO_2) and AuPt alloys onto Ni-Co hollow nanobox metal-organic frameworks (HNMs) (rGO-SnO_2/HNMs/AuPt), to yield an electroactive matrix material. Among the variety of nanomaterials, hollow nanostructures, which have higher surface-to-volume ratios and unique structural features, have shown great promise as electrode materials (Li et al. 2016; Yu et al. 2016). Therefore, hollow nanomaterials are extensively used for signal amplification and improvement of the sensitivity of electrochemical immunosensors. Ni-Co hollow nanoboxes are a new type of host matrixes that show a high chemical reactivity and a large surface/volume ratio (Zhao et al. 2012). rGO-SnO_2 is considered a desirable material that can provide a large specific surface area to improve the electro-conductibility and increase the amount of substance that can be loaded (Wang

et al. 2015). Moreover, bimetallic alloys are of particular importance in catalysis because the addition of the second metal provides variations in chemical and physical properties, thus contributing to catalytic activity and chemical selectivity (Yu et al. 2017). Specifically, Pt-based bimetallic systems show significantly improved catalytic and electrocatalytic activities. In particular, AuPt alloy nanoparticles show a greater catalytic activity and enhanced functionalities compared to pure Pt and pure Au nanoparticles (Manivannan et al. 2017). Therefore, HNMs/AuPt was combined with rGO-SnO_2, as the basic materials, to further enhance the surface area and facilitate electron transfer. In this system, AuPt alloys were chosen not only as the linkers between the substrate materials and adsorbed substances, but also as linkers between the nanoboxes and rGO-SnO_2. To further increase the sensitivity of the immunosensor, considerable efforts have been devoted to immobilise more of the target LAG-3 protein in the sandwich-type immunosensor. The biotin-streptavidin system was selected owing to its high specificity and the strong affinity of streptavidin for biotin. The choice of this system was also based on the fact that a single molecule of streptavidin can combine with four biotin molecules, exhibiting an efficient streptavidin-biotin interaction (Yang et al. 2014). Therefore, biotin-modified antibodies (Bio-Ab_1) could be efficiently immobilised on the sensing platform surface through the highly selective recognition of the biotin-streptavidin system, to thus achieve improved sensitivity. Therefore, we utilised rGO-SnO_2/HNMs/AuPt nanocomposite materials, which served as a good carriers and bridges, and the biotin-streptavidin system, for the efficient immobilisation of the detection protein, to improve the sensitivity and selectivity of the immunosensor.

As the most used and classic analytical model, the sandwich-type structure has been widely applied to clinical disease diagnosis owing to its outstanding convenience,

ultrasensitivity, and selectivity when used in electrochemical immunosensors (Chen et al. 2016; Gao et al. 2017; Wang et al. 2017a). In the typical sandwich-type electrochemical sensor, multifunctional nanomaterials serve as the label, and the fabrication of labelled secondary antibodies (Ab_2) was used to achieve signal amplification with good electrochemical characteristics (Wang et al. 2015). With the increase in antigen concentration, the number of labels conjugated with Ab_2 will increase accordingly, resulting in enhancement of the electrochemical signal and an enhancement in the sensitivity of the immunosensor. Obviously, the label acts as the crucial factor for enhancing the sensitivity in the traditional sandwich-type immunosensor. However, the specific recognition between the antibodies and antigens can generate a hydrophobic and insulating layer on the modified electrode and hinder the electron transfer (Fan et al. 2014). Therefore, the sensitivity may be limited to some extent.

In this study, to achieve the measurement of low concentrations of the LAG-3 protein, a signal-decreased label with inferior electron transfer ability and inferior electrocatalytic activity can be used to enhance the electrochemical signal change. Silicon dioxide (SiO_2) has attracted wide attention not only because of its uniform size, high biocompatibility, low toxicity, and low cost in biological applications (Z et al. 2015), but also because it possesses a large steric hindrance, weak electron transferability, and inferior electrocatalytic activity (Wang et al. 2015). Therefore, SiO_2 was used as the label to be conjugated with Ab_2. Both the obtained conjugate (SiO_2-Ab_2) and antigen can facilitate the decrease of the electrocatalytic current response, increase the current-difference, and contribute to enhancing the sensitivity of the designed immunosensor.

Herein, a type of sandwich enzyme-free electrochemical immunosensor was

developed by encapsulating rGO-SnO_2/HNMs/AuPt nanocomposite materials, to yield an electroactive matrix material, and the signal amplification tag, SiO_2-Ab_2, on the immunosensor, to further increase its sensitivity. First, the matrix was coated directly on the glassy carbon electrode (GCE) surface to produce the electrochemical signal. For the immobilisation of Bio-Ab_1 and further enhancement of the sensitivity of our immunosensor, we integrated streptavidin into the sensor by exploiting the amino-Au and amino-Pt affinity. It is well-known that the high affinity between streptavidin and biotin is beneficial for the capture of specific classes of proteins (Yang et al. 2017). Via the antigen-antibody reaction, SiO_2-Ab_2 was coated on the immunosensor to enhance its sensitivity. Finally, the proposed biosensor amplified the electrochemical signals by the reduction of H_2O_2, to yield an excellent electrochemical signal response. The proposed enzyme-free sandwich immunosensor showed a high sensitivity for the quantitative determination of the LAG-3 protein in human serum and a considerable potential for the detection of the LAG-3 protein for clinical diagnoses.

2. Experimental Methods

2.1. Reagents and chemicals

LAG-3 ELISA kit was purchased from Cusabio Co., Ltd. (Wuhan, China). LAG-3 protein was purchased from Cloud-Clone., Ltd. (Wuhan, China). Monoclonal anti-LAG-3 antibodies were purchased from Sangon Biotech Co., Ltd. (Shanghai, China). Gold chloride ($HAuCl_4 \cdot 4H_2O$), bovine serum albumin (BSA), chloroplatinic acid (H_2PtCl_6), (3-Aminopropyl) triethoxysilane (APTES), and sodium borohydride ($NaBH_4$) were purchased from Sigma-Aldrich Chemical (St. Louis, USA,

www.sigmaaldrich.com). rGO-SnO_2 was obtained from Nanjing XFNANO Materials TECH Co., Ltd. (China). The characterisation of graphene oxide and reduced graphene oxide from the supplier is provided in Supplementary Information S1. 2-Methylimidazole, cobalt nitrate hexahydrate ($Co(NO_3)_2 \cdot 6H_2O$), cetyltrimethyl ammonium bromide (CTAB), nickel nitrate hexahydrate ($Ni(NO_3)_2 \cdot 6H_2O$), and silicon dioxide (550 nm) were purchased from Aladdin Biochemical Technology Co., Ltd.

The buffer solutions involved in this study are as follows: 0.2 M phosphate buffer (pH 6.8) containing 0.1 M Na_2HPO_4, 0.1 M KH_2PO_4, and 0.1 M KCl was utilised as the working buffer; LAG-3 membrane protein solubilisation buffer (pH 8.0) containing 20 mM Tris, 150 mM NaCl, 1 mM EDTA, 1 mM DTT, 0.01% sarcosyl, 5% Trehalose, and Proclin 300; and the LAG-3 protein dilution buffer utilised was 0.2 M phosphate buffer. All other reagents were of analytical grade and used without further purification. All aqueous solutions were prepared using Millipore-Q water (≥ 18 MΩ·cm).

2.2. Apparatus and characterisation

Electrochemical measurements, including chronoamperometry (i-t), cyclic voltammetry (CV), and electrochemical impedance spectroscopy (EIS), were all performed on an AUTOLAB PGSTAT302 N electrochemical workstation (METROHM AUTOLAB B.V., The Netherlands), with a conventional three-electrode configuration. It consisted of a platinum wire as the auxiliary electrode, Ag/AgCl (with 3 M KCl) as the reference electrode, and a 3-mm diameter GCE modified by rGO-SnO_2/HNMs/AuPt were purchased from Gaoss union Technology Co., Ltd. (Wuhan, China), to be used as the working electrode. Field emission scanning

electron microscopy (FE-SEM) images were obtained using a Hitachi S4800 (Hitachi Limited, Japan) equipped with EX-250 Energy-dispersive X-ray spectroscopy (EDX, HORIBA Co., Japan, at an acceleration voltage of 10 kV). Transmission electron microscope (TEM) images were obtained from a JEM-2100F microscope (Japan) at an acceleration voltage of 200 kV. The powder X-ray diffraction (PXRD) patterns were collected with a D8 Advance X-ray diffractometer (Bruker Co., Germany) using Cu $K_{\alpha 1}$ radiation (λ = 0.154056 nm), with $2\theta = 5°$ to 90° (40 kV, 150 mA), and a scan speed of 10°/min. UV-vis measurements were carried out by using a Lambda 35 UV/vis Spectrometer (Perkin-Elmer, United States). Ultrasonic Cleaners using a SB 25-12 DTN (600W) were purchased from Ningbo Scientz Biotechnology Co., Ltd (Zhejiang, China).

2.3. Synthesis of the ZIF-67 nanocubes and Ni-Co LDH hollow nanoboxes

The Co-based zeolitic imidazolate framework (ZIF-67) nanocubes and Ni-Co-layered double hydroxide (Ni-Co LDH) hollow nanoboxes were synthesised through a surfactant-mediated method according to a previous report (He et al. 2017) with minor modifications. $Co(NO_3)_2 \cdot 6H_2O$ (58 mg) was dissolved in 2 mL of ultrapure water containing 3 mg of CTAB. Then, this solution was rapidly injected into 14 mL of an ultrapure aqueous solution containing 908 mg of 2-methylimidazole, with the colour of the solution changing immediately from colourless to purple; this solution was stirred at room temperature for 20 min. The product was collected by centrifugation and washed with ethanol at 10000 rpm for 10 min; this cycle was performed six times in order to remove the excess reactants.

The Ni-Co LDH hollow nanoboxes were synthesised as follows: 30 mg of ZIF-67

nanocubes was dispersed into 20 mL of ethanol. Then, 5 mL of an ethanol solution containing 50 mg of $Ni(NO_3)_2$ was added. The mixture was then stirred for 1 min. Subsequently, the reaction vessel was placed into an ultrasonic bath (the power of the ultrasonicator is 600 W) for 90 min. Subsequently, the product was centrifuged at 8000 rpm for 5 min, washed six times with 10 mL of ultrapure water to remove the unreacted chemicals, and then dried at 70°C. Then, 20 mg of the products was dispersed in 20 mL of deionised water. The mixed solution was heated to 85°C until the purple colour disappeared. Finally, the products were washed several times using ethanol and dried at 70°C overnight.

2.4. Synthesis of the hollow nanobox AuNPs (HNMs/Au), hollow nanobox-MOFs/AuPt alloys (HNMs/AuPt), and rGO-SnO_2/HNMs/AuPt

To synthesise the HNMs/AuPt (Ye et al. 2016), 10 mg of hollow nanoboxes were dispersed into 10 mL of ultrapure water, vigorously shaken for 2 min, and then sonicated for 1 h to obtain a homogeneous solution. Then, 10 mL of $NaBH_4$ ethanol solution (0.05 $mol \cdot L^{-1}$) was added to this mixture. After stirring for 20 min, 5 mL of a 1% H_2PtCl_6 ethanol solution and 5 mL of a 1% $HAuCl_4$ ethanol solution was added drop-wise into the solution and the solution was sonicated for 30 min. Then, 2 mL of $NaBH_4$ ethanol solution (0.05 $mol \cdot L^{-1}$) was added drop-wise to the solution, and the solution was sonicated for 30 min. Finally, the product was centrifuged at 8000 rpm for 5 min and washed thrice with ultrapure water and dried at 70°C. The method for the synthesis of the HNMs/Au was the same as that for the synthesis of the HNMs/AuPt, except that 5 mL of 1% $HAuCl_4$ ethanol solution was used instead of 5 mL of 1% H_2PtCl_6; the same method was used for the synthesis of HNMs/Pt (using 5 mL of 1% H_2PtCl_6 solution). The detailed procedures for the synthesis of the

rGO-SnO_2/HNMs/AuPt and label signal rGO-SnO_2 are provided in **Supplementary Information S2 and S3**, respectively.

2.5. Fabrication of the electrochemical immunosensor

The fabrication procedure of the electrochemical immunosensor is outlined in **Scheme 1**. The bare GCEs were polished repeatedly into mirrors using both 0.3- and 0.05-μm alumina slurries. Then, the GCEs were washed ultrasonically in ultrapure water and absolute alcohol, and again in ultrapure water for several minutes. After drying in nitrogen at room temperature, 5 μL of the 2 $mg{\cdot}mL^{-1}$ rGO-SnO_2/HNMs/AuPt nanocomposite material was dropped onto the surface of the GCE, and dried in nitrogen. Subsequently, 10 μL of streptavidin (500 $ng{\cdot}mL^{-1}$) was coated onto the modified electrode surface; the streptavidin combined with the AuPt alloys via Au-NH_2 and Pt-NH_2 bonds. The electrode was stored at 4°C overnight to allow the streptavidin to more efficiently combine with the rGO-SnO_2/HNMs/AuPt. After the reaction, the electrode was thoroughly rinsed with a 0.2 M phosphate buffer (pH 6.8) solution to remove unsolidified bound reactants and was then dried in nitrogen. Next, 10 μL of biotin-modified antibodies (Bio-Ab_1) (2 $\mu g{\cdot}mL^{-1}$) was added onto the electrode surface for 1 h at 37°C, resulting in the immobilisation of Bio-Ab_1 on the modified electrode due to the streptavidin-biotin affinity (Yin et al. 2017). After washing as described above, the electrode was blocked with 6 μL of BSA solution (1%, w/v) for 30 min at 37°C to block the nonspecific adsorption.

2.6. Electrochemical measurement

According to the typical procedures for the sandwich-type immunoassay, 10 μL of LAG-3 protein standard solutions with different concentrations ranging from 10 $pg \cdot mL^{-1}$ to 1 $\mu g \cdot mL^{-1}$ were dropped onto the modified electrode for 60 min at 37°C. After thorough rinsing with PBS, 10 μL of the SiO_2-Ab_2 was dropped onto the electrode, which was then incubated for another 60 min. After washing with PBS at least thrice to rinse off the unbound SiO_2-Ab_2, the electrodes were subjected to electrochemical measurements. The amperometric i-t curves were recorded at -0.4 V in 8 mL of a working buffer solution (pH = 6.8) at room temperature. After the background current was stabilised, 10 μL of H_2O_2 (3 $mmol \cdot L^{-1}$) was added to the solution and the electrochemical signal changes were recorded.

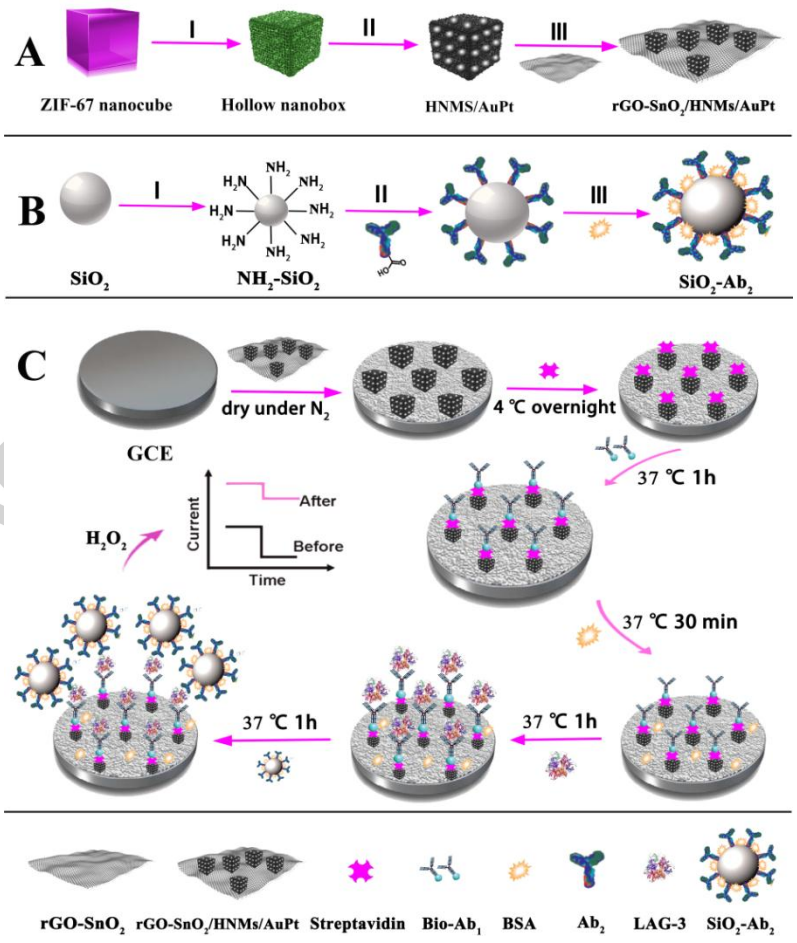

Scheme 1. (A) Preparation of rGO-SnO_2/HNMs/AuPt: I)reaction of ZIF-67 nanocubes with $Ni(NO_3)_2$ in an ultrasonic bath and heated to 85°C to form Ni-Co LDH nanoboxes at room temperature; II) reaction of Ni-Co LDH nanoboxes with $HAuCl_4$ and H_2PtCl_6 via $NaBH_4$ reduction to form HNMs/AuPt; and III) Stirring the HNMs/AuPt solution with rGO-SnO_2 overnight at room temperature. (B) Preparation of SiO_2-Ab_2: I) reaction of SiO_2 with APTES under magnetic stirring at 70°C for 1.5 h to form NH_2-SiO_2; II) NH_2-SiO_2 combined with anti-LAG-3 antibodies using EDC/NHS in 4°C overnight; and III) BSA was added to block the remaining active sites for 12 h at 4°C. (C) Schematic illustration of the stepwise assembly procedure of the sandwich electrochemical immunosensor interface.

3. Results

3.1. Characterisation of different nanomaterials

The morphology of the synthesised nanocomposite was characterised by FE-SEM and TEM. As shown in **Fig. 1A**, the obtained nanocubes had smooth surfaces and were uniform, with an average diameter of approximately 200 nm. TEM images (**Fig. 1D**) verified the cubical shape of the nanocubes. The energy dispersive X-ray (EDX) pattern (**Figure S1a**) confirmed the formation of ZIF-67 nanocubes. After reaction with an appropriate amount of $Ni(NO_3)_2$ for 90 min at 25°C, the solid nanocubes were converted into nanoboxes. Typical FE-SEM images shown in **Fig. 1B** indicate that the solid morphology of the particles and the size of the precursor ZIF-67 nanocubes were preserved (**Fig. 1E**). The EDX spectrum (**Figure S1B**) reveals the existence of an Ni element, showing that Ni was incorporated into the nanoboxes. When the AuPt NPs were formed on the surface of the nanoboxes, the FE-SEM image (**Fig. 1C**) indicated that the edge of the nanoboxes obviously collapsed and was thickened, with the presence of granular material. The TEM image presented in **Fig. 1F** suggested that the orbicular particulate AuPt NPs were attached to the edges of the cubic boxes. EDX (**Fig. S1C**) showed that the characteristic elements of the granular material on the edge of the frame contained Au and Pt simultaneously, proving that the granular material is the AuPt alloy. Examination of the EDX image (**Fig. S1D**) showed that characteristic elements of Au, Pt, Co, Ni, C, O, and N could be observed, implying the

successful loading of AuPt alloys onto the nanoboxes. As shown in **Fig. 1G**, the wrinkled paper-like structure with small round metal particles of rGO-SnO_2 was validated, and may provide a large surface area for modification by the AuPt alloy hollow nanoboxes. EDX (**Fig. S1E**) showed the characteristic elements of C, O, and Sn. As seen in **Fig. 1H**, after rGO-SnO_2-APTES was stirred with the HNMs/AuPt, the wrinkled paper-like structure was distinctly attached to several cubic solids. Examination of the EDX image (**Fig. 1I**) showed characteristic elements of Sn, Au, Pt, Co, Ni, C, O, and N, confirming the successful loading of HNMs/AuPt onto the rGO-SnO_2-APTES. The characterisation of powder X-ray diffraction (PXRD) of different nanomaterials is shown in **Supplementary Information S4**. The SEM image and UV-vis spectra of SiO_2, Ab_2, and SiO_2-Ab_2 are shown in detail in **Supplementary Information S5**.

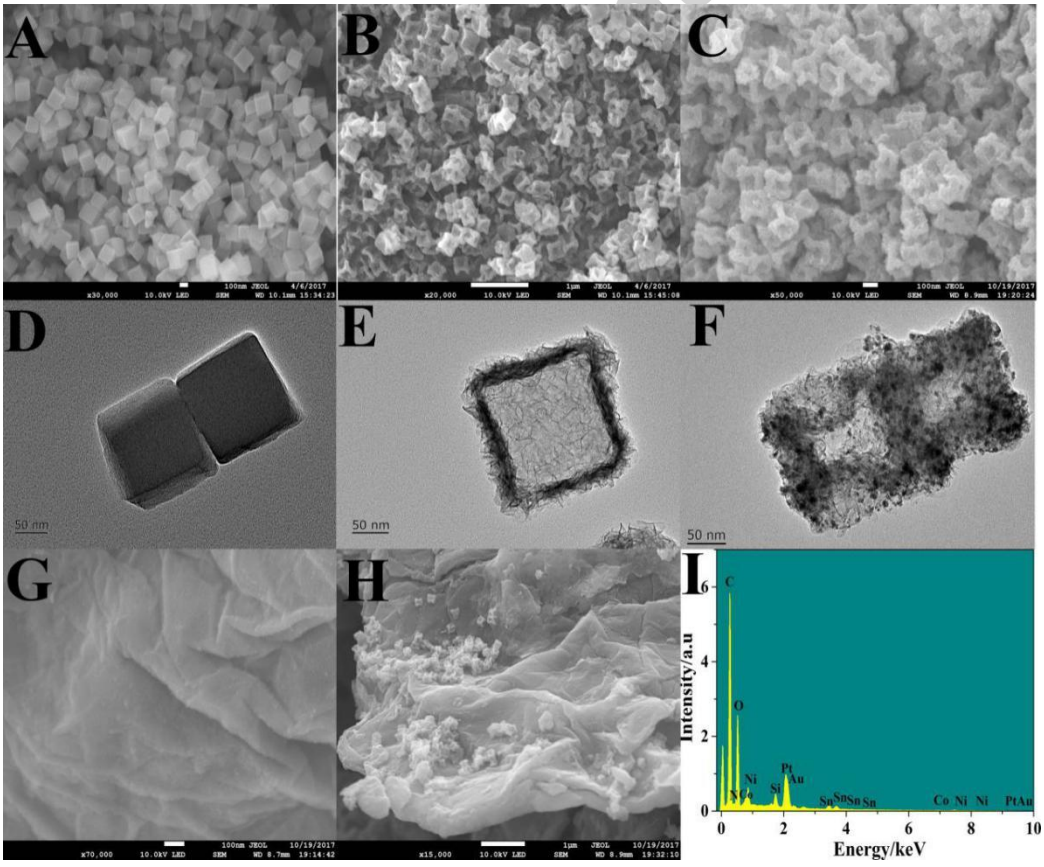

Fig. 1. FE-SEM image of ZIF-67 (A), Ni-Co LDH (B), and HNMs/AuPt (C). TEM image of ZIF-67 (D), and Ni-Co LDH HNMs (E), and HNMs/AuPt (F), FE-SEM image of rGO-SnO_2 (G) and rGO-SnO_2/HNMs/AuPt (H). EDX image of rGO-SnO_2/HNMs/AuPt (I).

3.2. Electrochemical characterisation of the stepwise-modified electrode

I-t curves for the electrode after different stepwise modifications were performed are shown in **Fig 2A**. Since bare GCE does not have the ability to catalyse H_2O_2, the electrochemical signal response was absent when H_2O_2 was introduced into the working buffer (curve a). Owing to the fact that the rGO-SnO_2/HNMs/AuPt substrate material could promote the electron transfer and catalysed H_2O_2, the electrochemical signal response increased visibly after the immobilisation of rGO-SnO_2/HNMs/AuPt onto the electrode (curve b). Next, the electrochemical signal response decreased after non-electroactive streptavidin was captured on the surface of electrode (curve c). Then, as expected, the response signal decreased after Bio-Ab_1 coating (curve d).

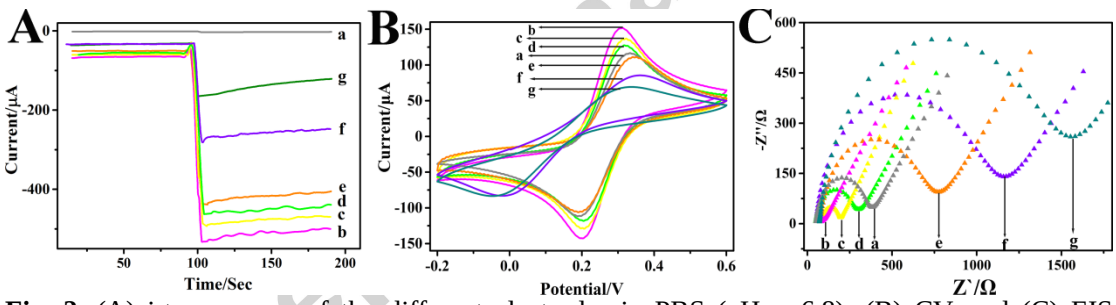

Fig. 2. (A) i-t responses of the different electrodes in PBS (pH = 6.8); (B) CV, and (C) EIS characterisation of electrodes at various steps of modification in a 5 mM $[Fe(CN)_6]^{3-/4-}$ solution: (a) bare GCE, (b) rGO-SnO_2/HNMs/AuPt, (c) streptavidin/rGO-SnO_2/HNMs/AuPt, (d) Bio-Ab_1/ streptavidin/rGO-SnO_2/HNMs/AuPt, (e) BSA/Bio-Ab_1/streptavidin/rGO-SnO_2/HNMs/AuPt, (f) LAG-3/BSA/Bio-Ab_1/streptavidin/rGO-SnO_2/HNMs/AuPt, and (g) SiO_2-Ab_2/LAG-3/BSA/Bio-Ab_1/streptavidin/ rGO-SnO_2/HNMs/AuPt

Non-conductive BSA, which was the blocking agent, caused the electrochemical signal response to decrease again (curve e). Moreover, the electrochemical signal response further decreased after incubation with LAG-3, which possessed negative charges (curve f), accounting for the successful specific binding. Finally, incubation of the SiO_2-Ab_2 signal label led to a significant decrease in the electrochemical signal

response. The reason for this is that signal labels have a large steric hindrance and an inferior ability to catalyse H_2O_2 (curve g).

CV and EIS measurements were performed step-by-step to examine the interfacial properties of the modified electrodes during fabrication in a 5-mM $[Fe(CN)_6]^{3-/4-}$ solution containing 0.1 M KCl (as shown in **Fig. 2B and Fig. 2C)**. The description of CV and EIS measurements are given in **Supplementary Information S6.**

3.3. Mechanism of signal amplification strategy

Sensitivity is strongly related to the difference in the current signal and is significantly affected by the immunosensor conductivity (Tang et al. 2016). We have investigated the signal amplification strategies of the matrix in this immunosensor; the four substrate nanocomposites included: (a) hollow nanoboxes (b) HNMs/Au (c) HNMs/Pt and (d) HNMs/AuPt. As shown in **Fig. 3A**, compared to the biosensor incubated with hollow nanoboxes, the HNMs/Au exhibited a remarkable increase in the electrochemical signal, owing to the better ability of the AuNPs to catalyse the reduction of H_2O_2. When the immunosensor was incubated with HNMs/AuPt, the HNMs/AuPt alloys exhibited a much greater electrocatalytic current response than in case of the AuNPs and PtNPs. This demonstrates that AuPt alloys can vigorously catalyse the reduction of H_2O_2, causing the electrochemical signal to increase (**Fig. 3B**).

To investigate the signal amplification strategies of the biotin-streptavidin system in this immunosensor, control experiments using different nanomaterials for the reduction towards 3 mM H_2O_2 were carried out at -0.4 V in PBS (pH = 6.8). As shown in **Fig. 3C**, prior to the addition of streptavidin, a current difference of

approximately 80 μA was observed between the blank and 10 $\mu g \cdot mL^{-1}$ concentration of the LAG-3 protein. As shown in **Fig. 3D**, the current difference increased significantly to 180 μA when the immunosensor was combined with the biotin-streptavidin system, rather than when only the AuPt alloys were used. The sensitivity of the immunosensor also depends on the electrocatalytic current response change produced by the LAG-3 protein and SiO_2-Ab_2. Control experiment for the concentration of rGO-SnO_2/HNMs/AuPt (2 $mg \cdot mL^{-1}$) for the reduction towards 3 mM H_2O_2 was carried out at -0.4 V in PBS (pH = 6.8). As shown in **Fig. 3E**, when 10 $\mu g \cdot mL^{-1}$ of the LAG-3 protein was combined with Bio-Ab_1, the electrocatalytic current response decreased only by approximately 180 μA, when compared to the blank LAG-3 sample. However, after coating with the SiO_2-Ab_2, the current response change increased to approximately 280 μA (**Fig. 3F**).

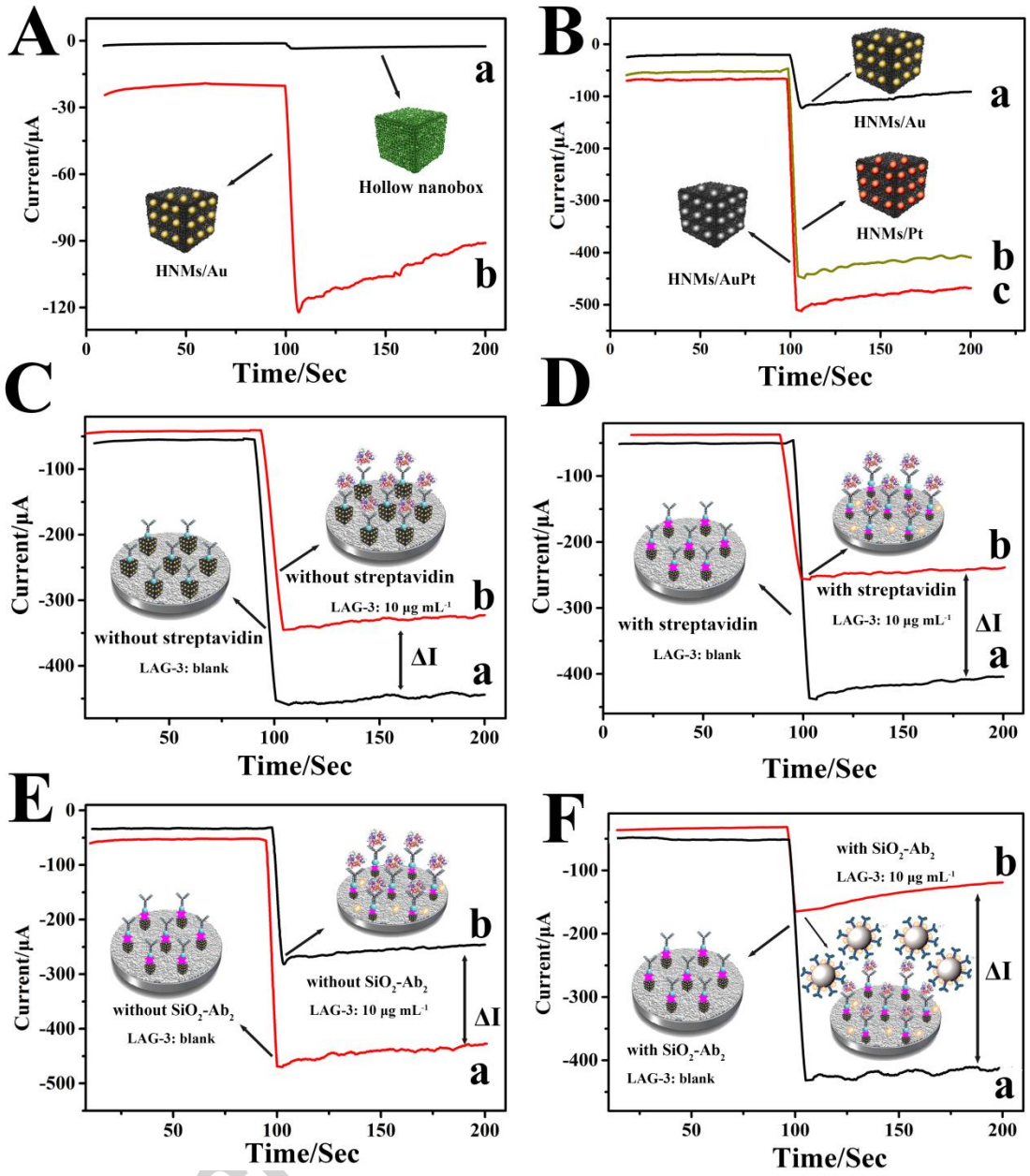

Fig. 3. The i-t curve of the prepared immunosensor incubated with different nanocomposite materials: (A) HNMs (a) and HNMs/Au (b); (B) HNMs/Au (a), HNMs/Pt (b), and HNMs/AuPt (c); (C) LAG-3 /BSA/ Bio-Ab_1/rGO-SnO_2/HNMs/AuPt: (a) LAG-3 (blank) and (b) LAG-3 (10 μg·mL^{-1}); (D) LAG-3/BSA/Bio-Ab_1/streptavidin/ rGO-SnO_2/HNMs/AuPt: (a) LAG-3 (blank) and (b) LAG-3 (10 μg·mL^{-1}); (E) LAG-3/BSA/Bio-Ab_1/streptavidin/ rGO-SnO_2/HNMs/AuPt: (a) LAG-3 (blank) and (b) LAG-3 (10 μg·mL^{-1}); and (F) SiO_2-Ab_2/LAG-3/BSA/Bio-Ab_1/rGO-SnO_2/HNMs/AuPt: (a) LAG-3 (blank) and (b) LAG-3 (10 μg·mL^{-1})

3.4. Optimisation of experimental conditions

Certain external experimental parameters influence the performance of the

proposed electrochemical immunosensor; therefore, to achieve the optimal immunosensor response, several parameters were optimised, including the following: the concentrations of the rGO-SnO_2/HNMs/AuPt, streptavidin, Bio-Ab_1, NH_2-SiO_2, and H_2O_2; the immobilisation time of the LAG-3; the pH of the supporting electrolyte; and the amount of AuPt alloys. As shown in **Fig. S4A**, the current response increased distinctly when the concentration of rGO-SnO_2/HNMs/AuPt increased from 1.0 mg·mL^{-1} to 2.0 mg·mL^{-1}, and then maintained a steady value. Hence, 2.0 mg·mL^{-1} was chosen as the optimal concentration.

Additionally, the streptavidin concentration is a critical factor for immobilising Bio-Ab_1 and influencing the immunosensor performance. Streptavidin concentration was tested in the 0.1–0.9 μg·mL^{-1} range. **Fig. S4B** shows that with an increased concentration of streptavidin, the current first decreased and then subsequently reached a plateau at 0.5 μg·mL^{-1}, suggesting that the amount of streptavidin reaches the maximum value on the surface of the immunosensor, based on the NH_2-Au and NH_2-Pt affinity for Au, PtNPs, and streptavidin. Therefore, 0.5 μg·mL^{-1} was selected as the optimal concentration of streptavidin.

Furthermore, the effect of Bio-Ab_1 concentration on the immunosensor response is shown in **Fig. S4C**. The current decreased significantly when the Bio-Ab_1 concentration changed from 1 μg·mL^{-1} to 2 μg·mL^{-1}, where it reached a plateau. This suggests that the amount of Bio-Ab_1 reaches its maximum value on the surface of the immunosensor through a combination with streptavidin. Hence, 2 μg·mL^{-1} was chosen as the optimal concentration of Bio-Ab_1.

The immobilisation time of the LAG-3 protein is a remarkably important parameter. The immobilisation time of LAG-3 was investigated and is shown in **Fig. S4D**. Accompanying the increase of the immobilisation time, the current decreased

quickly and remained steady at approximately 1 h, which was attributed to the antigen-antibody reaction, indicating that the maximum immobilisation of LAG-3 was obtained. To effectively bond SiO_2-Ab_2 in the following step, 1 h was chosen as the optimal incubation time.

The concentration of NH_2-SiO_2 is an important factor influencing the value of the electrocatalytic current response change. **Fig. S4E** shows the electrocatalytic current responses for different concentrations of NH_2-SiO_2 used as the label for the detection of 10 ng·mL^{-1} of LAG-3 in PBS at a pH of 6.8. As shown in this figure, the electrocatalytic current response persistently decreased from 1 mg·mL^{-1} to 3 mg·mL^{-1}, and the current remained steady. It is inferred that a greater amount of NH_2-SiO_2 was specifically bound to the electrode surface to hinder the electron transfer, leading to the gradually decreasing electrocatalytic current response. Therefore, 3 mg·mL^{-1} of NH_2-SiO_2 was selected as the concentration of the label throughout this study.

The pH value has a significant effect on the catalytic ability and the activity of biological proteins in the immunosensor. As shown in **Fig. S4F**, the current response of the immunosensor increased persistently with an increase in pH of the detection solution from 6.4 to 6.8, where it reached the maximum value. At a pH greater than 6.8, the current decreased distinctly. This is attributed to the decrease in bioactivity of the proteins under highly acidic or alkaline environments (Yang et al. 2017). Hence, a pH of 6.8 for the detection solution was selected as the optimised detection condition for the experiment.

The concentration of H_2O_2 is another important factor that influences the current response of the immunosensor. As shown in **Fig. S4G**, the current increased distinctly with an increase in the H_2O_2 concentration, and then, the current reached a plateau after the addition of 3 mmol·L^{-1} H_2O_2, illustrating the highest efficiency of

electrocatalysis at this point. Therefore, the optimal concentration of H_2O_2 was selected to be 3 mmol·L^{-1}.

The amount of PtNPs is also a significant factor influencing the catalytic efficacy of the electrochemical immunosensor. **Fig. S4H** shows that the current increased significantly with an increase in the amount of PtNPs and then remained steady with the addition of 5 mL of 1% H_2PtCl_6, which demonstrated that the quantity of PtNPs on the surface of the hollow nanoboxes has reached the saturated state. Therefore, 5 mL of H_2PtCl_6 (w/w, 1%) was selected as the optimal quantity.

3.5. Analytical performance of the electrochemical immunosensor

Under optimised experimental conditions, the effects of different concentrations of LAG-3 on H_2O_2-catalytic ability were examined using an amperometric i-t curve at -0.4 V in 8 mL of PBS (pH = 6.8) measured every 100 s. The relationship between the electrochemical signal towards the reduction of H_2O_2 and the concentration of LAG-3 is shown in **Fig. 4A**. The currents gradually decreased with increasing concentrations of the LAG-3 protein. Calibration plots between the electrochemical current signal response and the logarithm of LAG-3 protein concentration displayed a good linear relationship from LAG-3 concentrations of 0.01 ng·mL^{-1} to 1 μg·mL^{-1} (**Fig. 4B**), with a detection limit of 1.1 pg·mL^{-1} (based on 3σ) and fitted the linear regression equation $Y = -52.3027 \log C_{LAG\text{-}3} + 251.39$, with a correlation coefficient of R = 0.9998. The results indicated that the proposed electrochemical immunosensor could be utilised to detect LAG-3 quantitatively. To further exhibit how the advanced

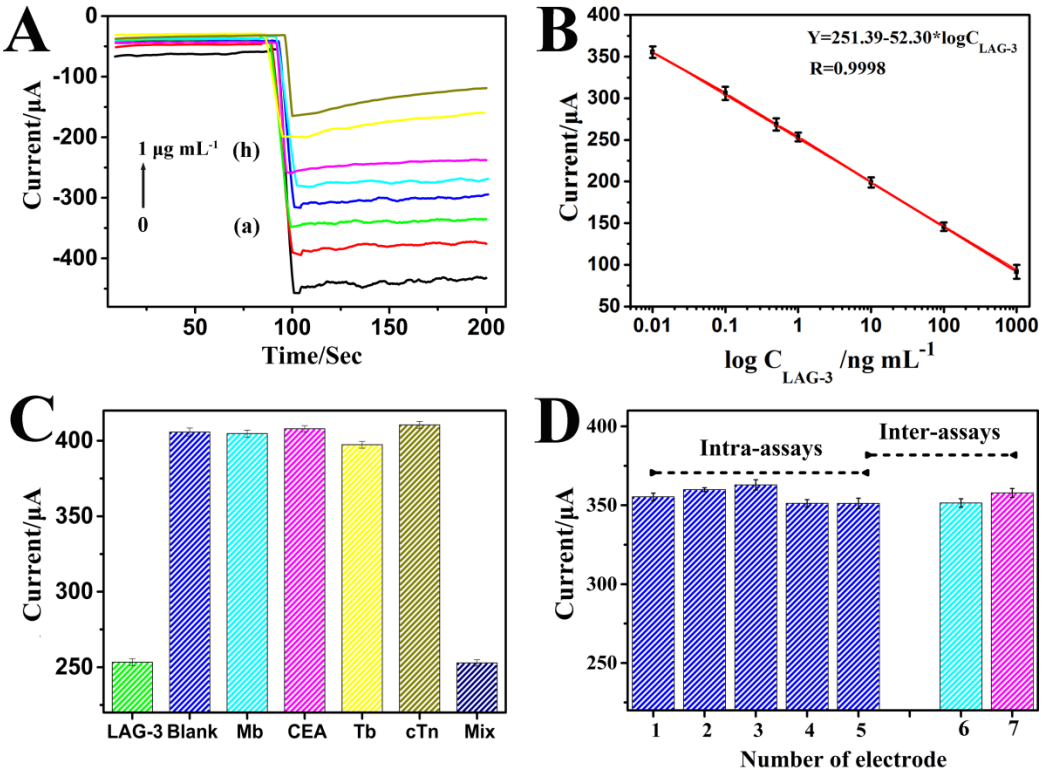

Fig. 4. (A) The i-t curve signals of the immunosensor for the determination of different concentration of LAG-3: (a) 0 ng·mL^{-1}, (b) 0.01 ng·mL^{-1}, (c) 0.1 ng·mL^{-1}, (d) 0.5 ng·mL^{-1}, (e) 1 ng·mL^{-1}, (f) 10 ng·mL^{-1}, (g) 100 ng·mL^{-1}, and (h) 1 μg·mL^{-1}. (B) The calibration curve of the biosensor for different concentrations of LAG-3 (n = 3). (C) Reproducibility of 7 different electrodes modified with 100 pg·mL^{-1} of LAG-3. (D) Specificity of the immunosensor towards 1 ng·mL^{-1} LAG-3, zero analyte, 100 ng·mL^{-1} Mb, 100 ng·mL^{-1} CEA, 100 ng·mL^{-1} Tb, 100 ng·mL^{-1} cTn, and a mixture of all these proteins.

nanomaterials work in synergy, we added two other calibrations plots, which were constructed using rGO-SnO_2/HNMs/Au and rGO-SnO_2/HNMs/Pt as the platform with the regression equation given in **Supplementary Information S7**. Furthermore, a performance comparison between the sandwich design-based MOF immunosensor and the other MOF electrochemical sensors in recent years is demonstrated in **Table S2**.

3.6. Specificity, stability, and reproducibility of the immunosensor

The specificity of the immunosensor was evaluated using 1 ng·mL^{-1} LAG-3 and

a 100-fold mass ratio of other proteins (100 ng·mL^{-1}), including carcinoembryonic antigen (CEA), thrombin (Tb), myohemoglobin (Mb), Cardiac troponin (cTn), and a mixture of all of the above-mentioned protein compounds (Mix). The current responses of each type are shown in **Fig. 4C**. First, the current responses of CEA, Tb, Mb, and Hb did not exhibit significant differences from the blank sample even when 100-fold higher concentrations of the proteins were added. Second, as seen in case of the current for the Mix, compared to only 1 ng·mL^{-1} LAG-3, the Mix current responses still did not show significant changes. These results indicate the non-specific interaction of other proteins. These foreign proteins had a negligible effect on the LAG-3 determination using the electrochemical immunosensor.

As shown in **Fig. 4D**, the reproducibility of the electrochemical immunosensor was evaluated for detecting LAG-3 with the concentrations of 10 pg·mL^{-1} using intra-assays and inter-assays. The RSD of the intra- and inter-assays were 1.47% and 1.27%, respectively. These results revealed that the assembled immunosensor exhibits an acceptable reproducibility. To evaluate the stability of the immunosensor, the fabricated sensors were stored at 4°C when not in use. As seen in **Fig. S6**, the currents showed no obvious differences during the first week of storage, and the current changes were smaller than 1.2%. After 4 weeks of storage, no apparent change for the determination of the same concentration of LAG-3 was detected, with 94.7% of the initial current response being retained, indicating that the designed biosensor had good stability.

Table 1. Determination of LAG-3 in human serum (n=3) with the proposed immunosensor

Samples	Added LAG-3 ($ng \cdot mL^{-1}$)	Found LAG-3 ($ng \cdot mL^{-1}$)	RSD (%)	Recovery (%)
1	0	0.008	2.03	0
2	0.05	0.052	1.31	104
3	0.5	0.49	1.77	99
4	5	5.16	1.53	103
5	50	48.46	2.07	97
6	500	541.57	2.19	108

3.7. Application for the analysis of serum samples

To evaluate the precision and accuracy of the proposed immunosensor in practical applications, various concentrations of the LAG-3 protein were added to 10-fold-diluted human serum samples (obtained from University-Town Hospital of Chongqing Medical University) to calculate the recovery rate by amperometric i-t curves. As seen in **Table 1**, the RSD ranged from 1.31% to 2.19%, and the recovery rate ranged from 97% to 108%.

4. Discussion

To the best of our knowledge, this is the first time that an electrochemical sensor has been used to detect the LAG-3 protein. We designed a highly sensitive electrochemical sensor. From the results of signal amplification in the comparative experiments (Fig. 3A–B), it was seen that the composites exhibited excellent electronic activity because of the structural advantages and superior conductivity of the MOFs. Simultaneously, the bimetallic alloys are of particular importance in catalysis because the addition of the second metal provides variations in chemical and physical properties, thus contributing to catalytic activity and chemical selectivity. Similarly, comparative experiments (Fig. 3C–D) demonstrated that the

biotin-streptavidin system improves the sensitivity of the proposed sandwich-type immunosensor, owing to the fact that streptavidin provides abundant active sites for the immobilisation of the Bio-Ab_1 as a signal amplification unit. Furthermore, signal-decreased label SiO_2-Ab_2 produces a more sensitive influence on the electrocatalytic signal response (Fig. 3E–F), because it can provide a large steric hindrance and suppress the electron transfer more effectively.

From the linear relationship between the electrochemical signal and LAG-3 concentration, we observed that the immunosensor achieved a wider linear dynamic range with an acceptable detection limit compared to other existing MOF-based sensors. Herein, we used the chronoamperometry method to detect the current response, which is more suitable for measuring the catalytic properties of nanocomposites compared to DPV and EIS. The detection limit of this work for LAG-3 protein determination seems to show fewer advantages than the method described by (Shen et al. 2015). However, compared with their method, the linear ranges of our method were superior to those of other methods. In addition, we have listed a table of the optimisation processes and showed how each parameter affects the overall performance of the biosensor (refers to **Table. S1**).

By utilising the designed electrochemical sensor for the detection of actual samples, we found that the immobilised biosensor is feasible for the detection of the LAG-3 protein and could satisfy the requirements of practical analyses, thereby illustrating that our method has the potential to be used in the determination of biomarkers for clinical diagnoses. Furthermore, the substrate material can also be used for other electrochemical sensors, and for performing photochemical and fuel cell experiments.

5. Conclusions

In summary, we present an enzyme-free cooperative catalysis signal amplification strategy for the ultrasensitive electronic detection of the LAG-3 protein based on a signal-decreased label immunosensor which has a great electronic resistance. We quantitatively detected different concentrations of the LAG-3 protein by using i-t curves for measuring the current difference after H_2O_2 reduction. On one hand, rGO-SnO_2/HNMs/AuPt composites were first successfully synthesised; they exhibited excellent electrocatalytic activity because of their structural advantages and superior conductivity. On the other hand, the biotin-streptavidin system was used to increase the sensitivity of the proposed immunosensor. Furthermore, the utilisation of SiO_2 increased the distinction of the electrochemical signal. With these advantages, the proposed immunosensor exhibited a wide linear range of measurement, from concentrations of 0.01 ng·mL^{-1} to 1 μg·mL^{-1}, and a low detection limit of 1.1 pg·mL^{-1}, and satisfied the requirement for sensitivity, stability, and reproducibility for detecting low amounts of the LAG-3 protein in human serum. Therefore, our method has the potential for use in the determination of biomarkers for clinical diagnoses.

Acknowledgements

This research was supported by the National Natural Science Foundation of China (Grant Nos. 31071093, 31170129, and 31200064) and the Science and Technology Planning Project of Yuzhong District of Chongqing City, China (No. 20140119).

References

Andrews, L.P., Marciscano, A.E., Drake, C.G., Vignali, D.A., 2017. LAG3 (CD223) as a cancer immunotherapy target. Immunological Reviews 276(1), 80.

Chen, J., Yu, C., Zhao, Y., Niu, Y., Zhang, L., Yu, Y., Wu, J., He, J., 2016. A novel non-invasive detection method for the FGFR3 gene mutation in maternal plasma for a fetal achondroplasia diagnosis based on signal amplification by hemin-MOFs/PtNPs. Biosensors & Bioelectronics 91, 892.

Fan, G.C., Han, L., Zhu, H., Zhang, J.R., Zhu, J.J., 2014. Ultrasensitive Photoelectrochemical Immunoassay for Matrix Metalloproteinase-2 Detection Based on CdS:Mn/CdTe Cosensitized TiO2 Nanotubes and Signal Amplification of SiO2@Ab2 Conjugates. Analytical Chemistry 86(24), 12398-12405.

Gao, F., Fan, T., Ou, S., Wu, J., Zhang, X., Luo, J., Li, N., Yao, Y., Mou, Y., Liao, X., 2017. Highly efficient electrochemical sensing platform for sensitive detection DNA methylation, and methyltransferase activity based on Ag NPs decorated carbon nanocubes. Biosensors & Bioelectronics 99, 201.

Golden, D., Kolmakova, A., Sura, S., Vella, A.T., Manichaikul, A., Wang, X.Q., Bielinski, S.J., Taylor, K.D., Chen, Y.D.I., Rich, S.S., 2016. Lymphocyte activation gene 3 and coronary artery disease. Jci Insight 1(17), e88628.

He, P., Yu, X.Y., Lou, X.W., 2017. Carbon-Incorporated Nickel-Cobalt Mixed Metal Phosphide Nanoboxes with Enhanced Electrocatalytic Activity for Oxygen Evolution. Angewandte Chemie International Edition 56, 3897-3900.

He, Z., Zang, S., Liu, Y., He, Y., Lei, H., 2015. A multi-walled carbon nanotubes-poly(L-lysine) modified enantioselective immunosensor for ofloxacin by using multi-enzyme-labeled gold nanoflower as signal enhancer. Biosensors & bioelectronics 73, 85.

Jie, Z., Yang, X., Ding, L., Keen-Circle, K., Borlawsky, T.B., Ozer, H.G., Jin, R., Payne, P., Huang, K., 2010. Using gene co-expression network analysis to predict biomarkers for chronic lymphocytic leukemia. Bmc Bioinformatics 11(S9), S5.

Juno, J.A., Stalker, A.T., Waruk, J.L., Oyugi, J., Kimani, M., Plummer, F.A., Kimani, J., Fowke, K.R., 2015. Elevated expression of LAG-3, but not PD-1, is associated with impaired iNKT cytokine production during chronic HIV-1 infection and treatment. Retrovirology 12(1), 17.

Kavosi, B., Salimi, A., Hallaj, R., Moradi, F., 2015. Ultra sensitive electrochemical immunosensor for PSA biomarker detection in prostate cancer cells using gold nanoparticles/PAMAM dendrimer loaded with enzyme linked aptamer as integrated triple signal amplification strategy. Biosens Bioelectron 74, 915-923.

Kim, S.S., Kim, S.H., Kang, H.S., Chung, H.Y., Choi, I., Cheon, Y.P., Lee, K.H., Lee, D.M., Park, J., Lee, S.Y., 2010. Molecular cloning and expression analysis of pig lymphocyte activation gene-3 (LAG-3; CD223). Veterinary Immunology & Immunopathology 133(1), 72-79.

Legat, A., Mabyel, H.H., Baumgaertner, P., Cagnon, L., Abedmaillard, S., Geldhof, C., Iancu, E.M., Lebon, L., Guillaume, P., Dojcinovic, D., 2015. Vaccination with LAG-3Ig (IMP321) and peptides induces specific CD4 and CD8 T-cell responses in metastatic melanoma patients - report of a phase I/IIa clinical trial. Clinical Cancer Research An Official Journal of the American Association for Cancer Research 22(6).

Li, B., Vanroey, M., Triebel, F., Jooss, K., 2008. Lymphocyte activation gene-3 fusion protein increases the potency of a granulocyte macrophage colony-stimulating factor-secreting tumor cell immunotherapy. Clinical Cancer Research An Official Journal of the American Association for Cancer

Research 14(11), 3545-3554.

Li, Z., Wu, H.B., Lou, X.W., 2016. Rational designs and engineering of hollow micro-/nanostructures as sulfur hosts for advanced lithium–sulfur batteries. Energy & Environmental Science 9(10).

Manivannan, S., Kang, I., Seo, Y., Jin, H.E., Lee, S.W., Kim, K., 2017. M13 Virus-Incorporated Biotemplates on Electrode Surfaces to Nucleate Metal Nanostructures by Electrodeposition. Acs Applied Materials & Interfaces.

Shapiro, M., Herishanu, Y., Katz, B.Z., Dezorella, N., Sun, C., Kay, S., Polliack, A., Avivi, I., Wiestner, A., Perry, C., 2017. Lymphocyte activation gene 3: a novel therapeutic target in chronic lymphocytic leukemia. Haematologica 102(5), 874.

Shen, W.-J., Zhuo, Y., Chai, Y.-Q., Yuan, R., 2015. Cu-Based Metal–Organic Frameworks as a Catalyst To Construct a Ratiometric Electrochemical Aptasensor for Sensitive Lipopolysaccharide Detection. Analytical Chemistry 87(22), 11345-11352.

Tang, Z., Wang, L., Ma, Z., 2016. Triple sensitivity amplification for ultrasensitive electrochemical detection of prostate specific antigen. Biosensors & Bioelectronics.

Topalian, S.L., Hodi, F.S., Brahmer, J.R., Gettinger, S.N., Smith, D.C., Mcdermott, D.F., Powderly, J.D., Carvajal, R.D., Sosman, J.A., Atkins, M.B., 2012. Safety, Activity, and Immune Correlates of Anti–PD-1 Antibody in Cancer. New England Journal of Medicine 366(26), 2443.

Turnis, M.E., Andrews, L.P., Vignali, D.A., 2015. Inhibitory receptors as targets for cancer immunotherapy. European Journal of Immunology 45(7), 1892-1905.

Wang, H., Chai, Y., Li, H., Yuan, R., 2017a. Sensitive electrochemiluminescent immunosensor for diabetic nephropathy analysis based on tris(bipyridine) ruthenium(II) derivative with binary intramolecular self-catalyzed property. Biosensors & Bioelectronics, 35-40.

Wang, H., Qi, C., He, W., Wang, M., Jiang, W., Yin, H., Ai, S., 2017b. A sensitive photoelectrochemical immunoassay of N 6 - methyladenosine based on dual-signal amplification strategy: Ru doped in SiO 2 nanosphere and carboxylated g-C 3 N 4. Biosensors & Bioelectronics 99, 281.

Wang, Y., Ma, H., Wang, X., Pang, X., Wu, D., Du, B., Wei, Q., 2015. Novel signal amplification strategy for ultrasensitive sandwich-type electrochemical immunosensor employing Pd-Fe3O4-GS as the matrix and SiO2 as the label. Biosensors & bioelectronics 74, 59.

Workman, C.J., Dugger, K.J., Vignali, D.A., 2002. Cutting edge: molecular analysis of the negative regulatory function of lymphocyte activation gene-3. Journal of Immunology 169(10), 5392-5395.

Xia, J., Ni, Z., Wang, J., Zhu, S., Ye, H., 2017. Overexpression of Lymphocyte Activation Gene-3 Inhibits Regulatory T Cell Responses in Osteoarthritis. Dna & Cell Biology.

Yang, Z., Lan, Q., Li, J., Wu, J., Yan, T., Hu, X., 2017. Efficient streptavidin-functionalized nitrogen-doped graphene for the development of highly sensitive electrochemical immunosensor. Biosensors & Bioelectronics 89(Pt 1), 312-318.

Yang, Z., Luo, S., Li, J., Shen, J., Yu, S., Hu, X., Dionysiou, D.D., 2014. A streptavidin functionalized graphene oxide/Au nanoparticles composite for the construction of sensitive chemiluminescent immunosensor. Analytica Chimica Acta 839, 67.

Ye, J., Cheng, B., Wageh, S., Alghamdi, A.A., Yu, J., 2016. Flexible Mg–Al layered double hydroxide supported Pt on Al foil for use in room-temperature catalytic decomposition of formaldehyde. Rsc Advances 6(41), 34280-34287.

Yin, H., Wang, H., Jiang, W., Zhou, Y., Ai, S., 2017. Electrochemical immunosensor for N6-methyladenosine detection in human cell lines based on biotin-streptavidin system and silver-SiO2 signal amplification. Biosensors & Bioelectronics 90, 494.

Yu, X.Y., Yu, L., Lou, X.W., 2016. Metal Sulfide Hollow Nanostructures for Electrochemical Energy Storage. Advanced Energy Materials 6(3).

Yu, Y., Yu, C., Niu, Y., Chen, J., Zhao, Y., Zhang, Y., Gao, R., He, J., 2017. Target triggered cleavage effect of DNAzyme: Relying on Pd-Pt alloys functionalized Fe-MOFs for amplified detection of Pb 2+. Biosensors & Bioelectronics.

Z, L., Y, W., Y, N., S, K., 2015. Fluorescence analysis of 6-mercaptopurine with the use of a nano-composite consisting of BSA-capped Au nano-clusters and core-shell Fe3O4-SiO2 nanoparticles. Biosensors & Bioelectronics 70, 246-253.

Zhao, M.Q., Zhang, Q., Huang, J.Q., Wei, F., 2012. Hierarchical Nanocomposites Derived from Nanocarbons and Layered Double Hydroxides - Properties, Synthesis, and Applications. Advanced Functional Materials 22(4), 675ived

Highlights

► An enzyme-free and sandwich immunosensor for tumour biomarkers lymphocyte activation gene-3 protein was designed.

►Hollow nanobox metal-organic frameworks (MOFs) functionalized reduced graphene oxide (rGO-SnO2), and gold and platinum alloys nanocomposites were synthesized and applied for the first time in an electrochemical immunosensor as matrix electroactive material.

► SiO_2 conjugate with antibody (SiO_2-Ab_2) was used as the signal label can facilitate the decrease of the electrocatalytic current response, and improve the sensitivity.